Supporting Information

Polypropylene separator-reinforced polymer-in-salt solid composite electrolytes for high-performance lithium ion batteries at room temperature

Kun Shi,*[a,b] Dawei Zheng,[a] Zhiming Guo,[a] Zeheng Yang [a] and Weixin Zhang *[a,b]

[a] School of Chemistry and Chemical Engineering, Hefei University of Technology, Hefei, Anhui, 230009, China

[b] Institute of Energy, Hefei Comprehensive National Science Center, Hefei, Anhui, 230031, China

E-mail: shikun@hfut.edu.cn (Kun Shi), wxzhang@hfut.edu.cn (Weixin Zhang)

Supplementary Figures S1-S14

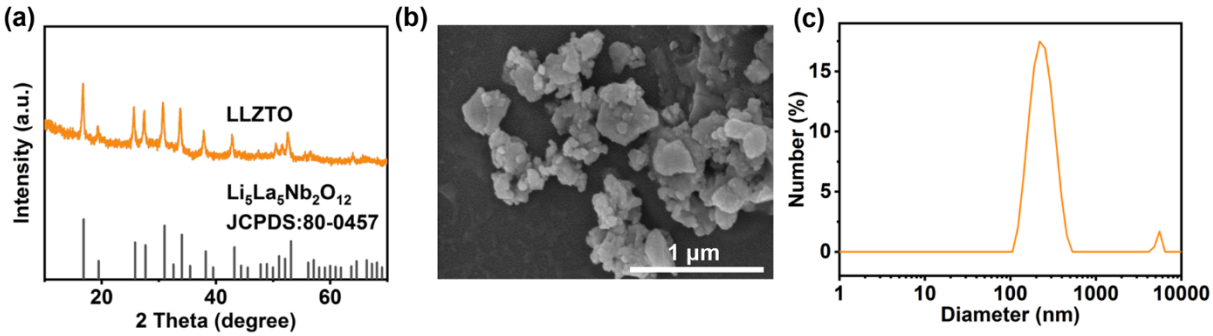

Fig. S1 (a) XRD pattern, (b) FESEM image and (c) size distribution of LLZTO.

Consistent with LLZO, the LLZTO incorporated in PVDF-Li-LZ SCEs or PVDF-Li-LZ SSCEs shows the pure cubic crystal structure in favor of high conductivity (Fig. S1a).[S1] A relatively uniform nanoscale characteristic belonging to LLZTO is demonstrated in the FESEM image (Fig. S1b), and the average particle size is located at around 242 nm (Fig. S1c).

Fig. S2 Photograph of PVDF-Li slurry (left) and PVDF-Li-LZ slurry (right).

In sharp contrast to the transparent PVDF-Li slurry, the PVDF-Li-LZ slurry dispersed with LLZTO particles exhibits a yellowish-brown color mainly owing to the LLZTO-induced structural modification of PVDF polymers (Fig. S2).[S2,S3]

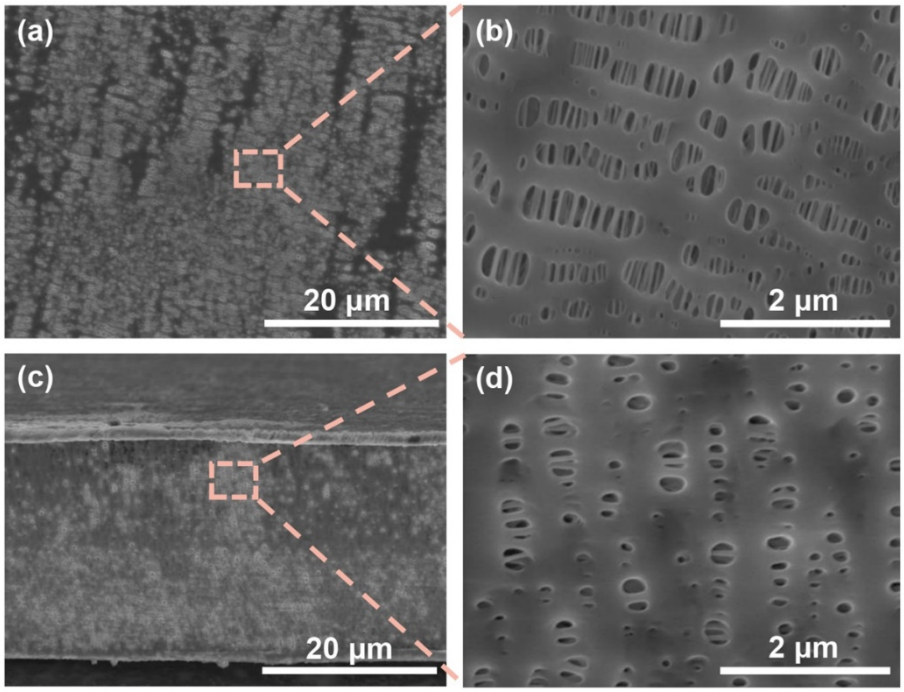

Fig. S3 (a, b) Top-view and (c, d) cross-sectional FESEM images of pristine PP separator.

Whether on the membrane surface (Fig. S3a and b) or cross section (Fig. S3c and d), abundant uniformly distributed nanoscale holes are clearly observed, which enables the construction of continuous three-dimensional nano channels for PVDF-Li-LZ slurry infiltration. In addition, it can be seen from Fig. S3c that, the pristine PP separator displays a thickness of approximately 25 μm equivalent to the product parameter.

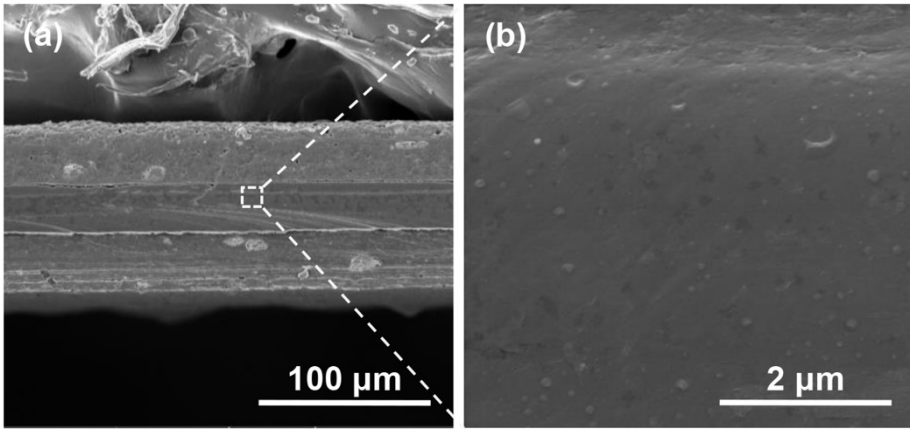

Fig. S4 (a) Cross sectional FESEM image of the as-prepared PVDF-Li-LZ SSCEs membrane and (b) corresponding enlarged view of the middle PP layer.

The cross sectional morphology of the as-prepared PVDF-Li-LZ SSCEs are more clearly observed at a higher magnification (Fig. S4). Obviously , no nanopores but only a dense plane can be found for the PP layer in PVDF-Li-LZ SSCEs (Fig. S4b), indicating that the original holes of porous PP separator are indeed fully filled during PVDF-Li-LZ slurry infiltration, rendering the continues pathways for ion transfer.

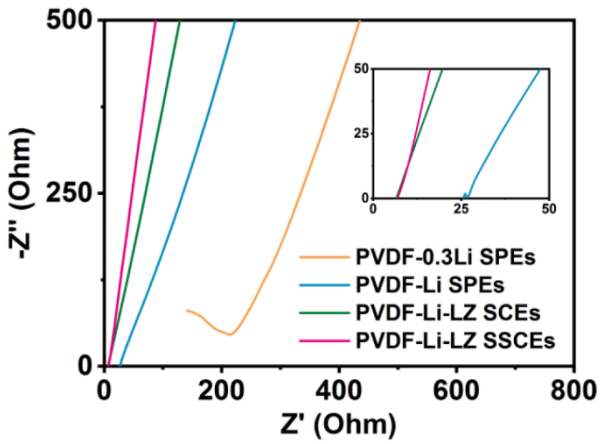

Fig. S5 Nyquist spectra of the stainless steel symmetrical cells with PVDF-0.3Li SPEs, PVDF-Li SPEs, PVDF-Li-LZ SCEs and PVDF-Li-LZ SSCEs at 25 °C.

According to the Nyquist spectra as shown in Fig. S5, the ionic conductivities of PVDF-0.3Li SPEs, PVDF-Li SPEs, PVDF-Li-LZ SCEs and PVDF-Li-LZ SSCEs are calculated as 2.31×10^{-5} S cm^{-1}, 1.94×10^{-4} S cm^{-1}, 7.54×10^{-4} S cm^{-1} and 7.16×10^{-4} S cm^{-1} at 25 °C, respectively.

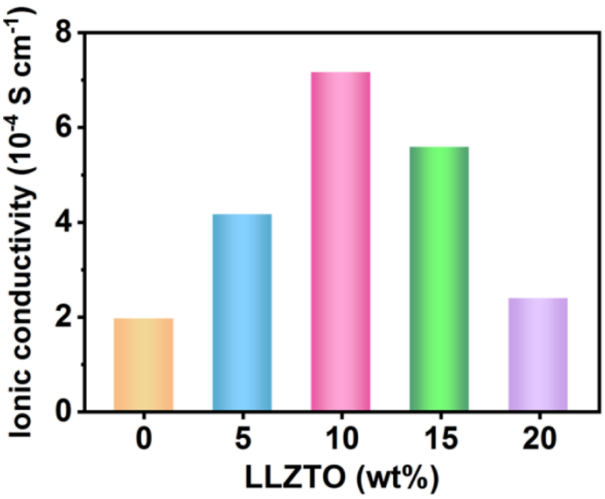

Fig. S6 LLZTO content-dependent ionic conductivity of PVDF-Li-LZ SSCEs at 25 °C.

Fig. S6 demonstrates that the LLZTO content has a significant effect on the performance of PVDF-Li-LZ SSCEs in ion conduction. As the mass fraction of LLZTO gradually increases, the ionic conductivity of PVDF-Li-LZ SSCEs increases first due to the reduced polymer crystallinity as well as the promoted dissociation of lithium salt, whereas then decreases when the LLZTO content exceeds 10 wt% because the excessively high nanofiller loading will inevitably lead a hazardous particle aggregation.[S4] Therefore, the 10 wt% content of LLZTO is selected in this work as an optimal value to achieve the maximum ionic conductivity of 7.16×10^{-4} S cm^{-1} of PVDF-Li-LZ SSCEs.

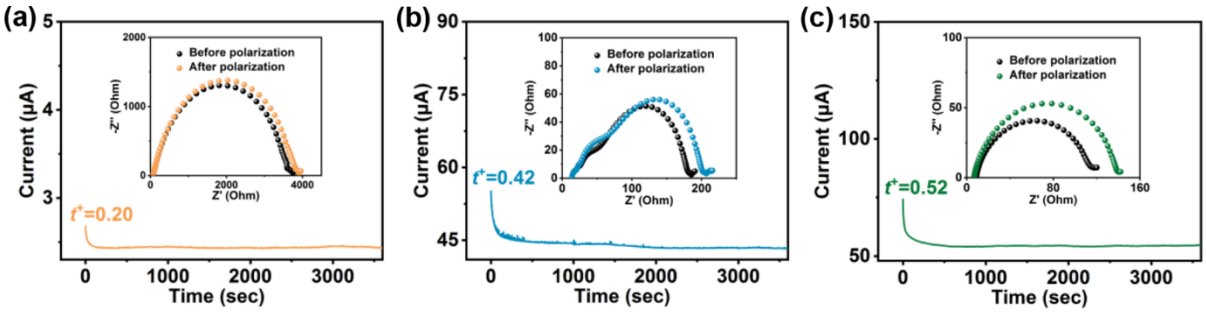

Fig. S7 DC polarization curves performed on the lithium symmetrical cells with (a) PVDF-0.3Li SPEs, (b) PVDF-Li SPEs, and (c) PVDF-Li-LZ SCEs.

As a key indicator reflecting the migration behavior of Li^+, the lithium-ion transference number (°) can be generally determined by the combined measurements of DC polarization and AC impedance (Fig. S7). Ascribed to the mobility restriction of $TFSI^-$ by the ion clusters,[S5] the polymer-in-salt PVDF-Li SPEs exhibit an increased t_{Li^+} of 0.42 than that of 0.2 belonging to PVDF-0.3Li SPEs (Fig. S7a and b). Moreover, a higher t_{Li^+} value up to 0.52 can be achieved with the further addition of LLZTO, which results from the Li^+-conducting property of ceramic filler and its trapping effect on TFSI ions (Fig. S7c).[S6]

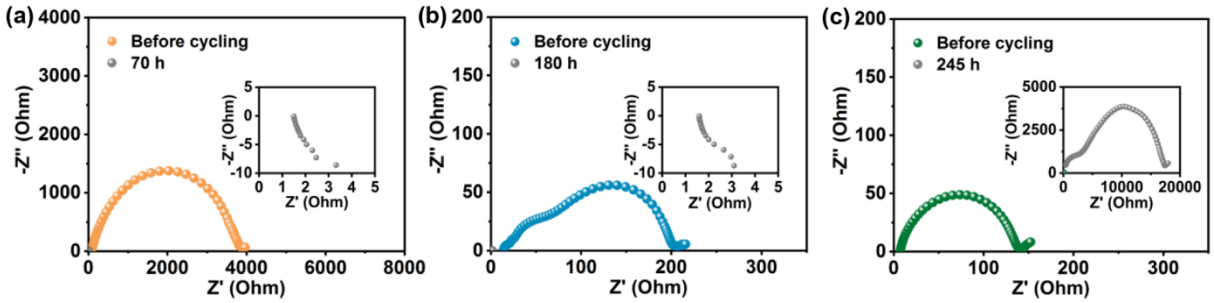

Fig. S8 Impedance spectra of the lithium symmetrical cells with (a) PVDF-0.3Li SPEs, (b) PVDF-Li SPEs, and (c) PVDF-Li-LZ SCEs.

In sharp contrast to that of Li|PVDF-Li-LZ SSCEs|Li cell, the impedance values of the Li|PVDF-0.3Li SPEs|Li and Li|PVDF-Li SPEs|Li cells decrease to zero after only 70 h and 180 h cycling respectively (Fig. S8a and b), whereas that of the Li|PVDF-Li-LZ SCEs|Li cell increases significantly from 131 Ω to 14993 Ω after 245 h cycling (Fig. S8c), all suggesting the interfacial instability between these three groups of control electrolytes and lithium anodes.

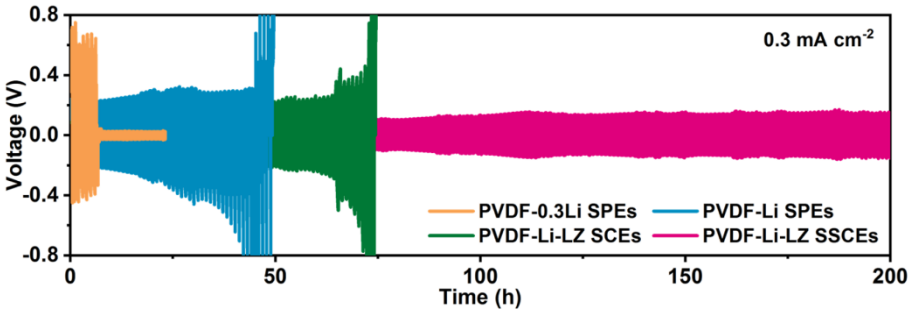

Fig. S9 Galvanostatic cycling performance of lithium symmetrical cells at 0.3 mA cm^{-2}.

Even at a high current density of 0.3 mA cm^{-2}, the PVDF-Li-LZ SSCEs still delivers an excellent electrochemical stability against lithium metal far superior to the other three electrolytes. As shown in Fig. S9, a long cell cycle life over 200 h accompanied by a negligible potential fluctuation within the range from -0.2 V to 0.2 V can be achieved for PVDF-Li-LZ SSCEs. While for the PVDF-0.3Li SPEs, PVDF-Li SPEs or PVDF-Li-LZ SCEs, the obvious cell failure would occur only after 7 h, 45 h or 72 h of charge-discharge operations, respectively.

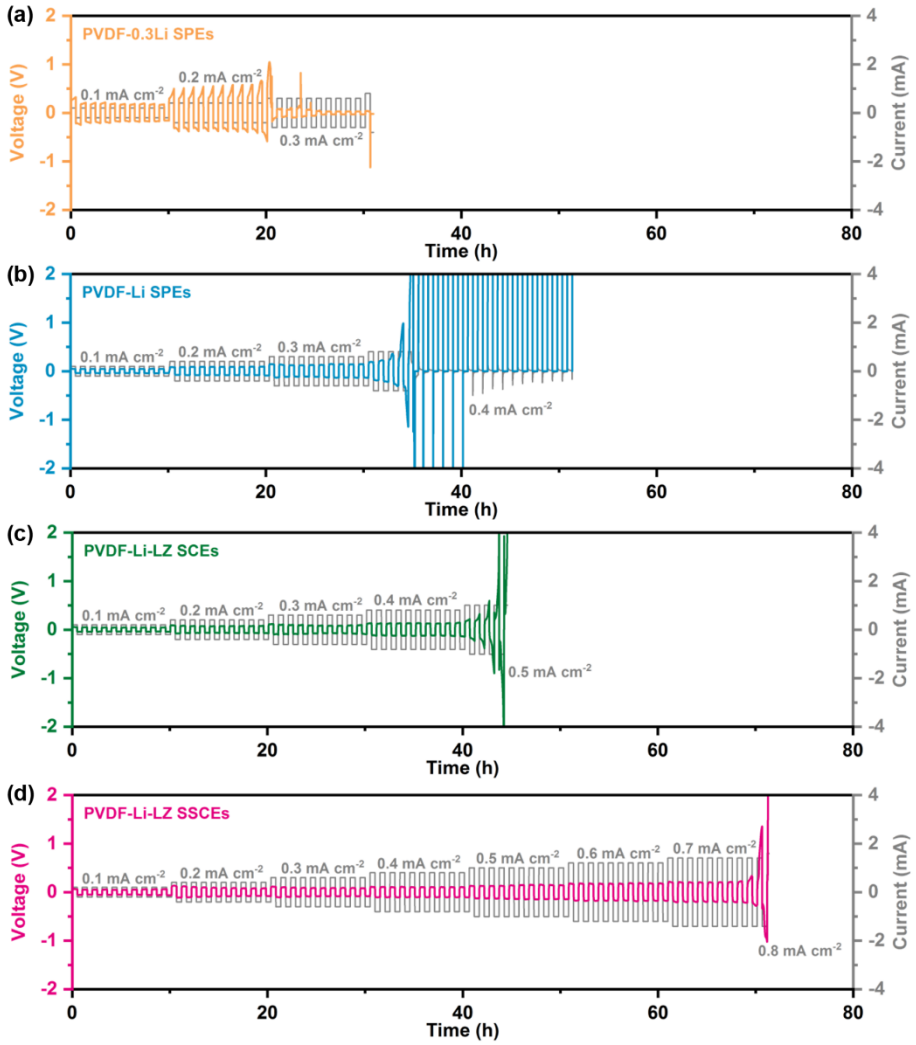

Fig. S10 Critical current density tests at various current densities for the lithium symmetrical cells with (a) PVDF-0.3Li SPEs, (b) PVDF-Li SPEs, (c) PVDF-Li-LZ SCEs and (d) PVDF-Li-LZ SSCEs, respectively.

The critical current density measurements are carried out to evaluate the maximal current density that these electrolyte membranes could tolerate before cell failure (Fig. S10). When the applied current density increases from 0.1 mA cm^{-2} to 0.8 mA cm^{-2} step by step, the sharp rise or rapid drop to zero of overpotential is observed for the Li|PVDF-0.3Li SPEs|Li, Li|PVDF-Li SPEs|Li and Li|PVDF-Li-LZ SCEs|Li cell at 0.3 mA cm^{-2}, 0.4 mA cm^{-2} and 0.5 mA cm^{-2}, respectively. In contrast, the Li/PVDF-Li-LZ SSCEs/Li cell achieves non sudden voltage variation until the current density rises up to 0.8 mA cm^{-2}. This result verifies the advantage of PVDF-Li-LZ SSCEs on the electrochemical compatibility towards lithium metal anodes among all the PVDF-based electrolyte membranes.

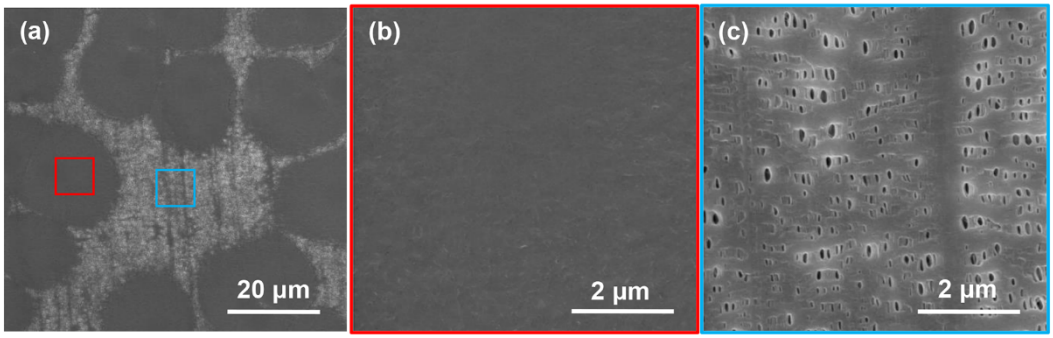

Fig. S11 Morphology of the PP-side surface of the pre-fabricated electrolyte membrane after unilateral coating on PP separator.

In order to make clear whether the PVDF-Li-LZ slurry penetrate through PP during the second coating or not, the surface morphology of the other side of the pre-fabricated electrolyte membrane after unilateral coating on PP separator is clearly characterized by SEM. As shown in Fig. S11, the PP separator after the first coating exhibits the partially filled porous structure on the uncoated side of PP separator (Fig. S11a,b), still with abundant nanoscale holes that are not completely filled by the PVDF-Li-LZ slurry (Fig. S11c). This result suggests that the PVDF-Li-LZ slurry during the next second coating process would penetrate into the above-mentioned nanoscale pores remaining in the once-coated PP separator and fully fill them. Therefore, the resultant integrated sandwich structure of PVDF-Li-LZ SSCEs can enable a good interface contact between the middle PP separator and the bilateral PVDF-Li-LZ layers for the excellent electrochemical performance.

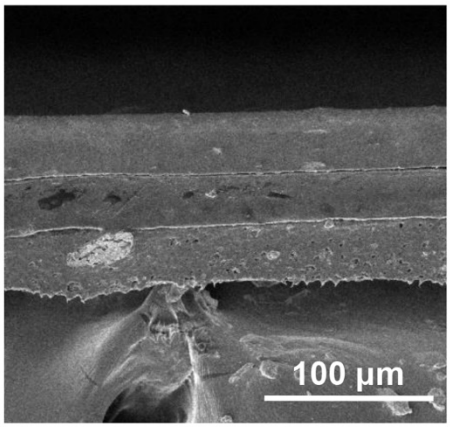

Fig. S12 Cross sectional FESEM images of the PVDF-Li-LZ SSCEs membrane after cell cycling at 0.3 mA cm^{-2} for 200 h.

It's precisely because the original holes of porous PP separator are fully filled with PVDF-Li-LZ electrolyte during PVDF-Li-LZ slurry infiltration, the PVDF-Li-LZ SSCEs membrane achieves an integrated structure with the PVDF-based layers tightly adhered on both sides of PP separator. As shown in Fig. S12, even after 200 h of cell cycling at 0.3 mA cm^{-2}, the middle PP separator and the bilateral PVDF-Li-LZ layers always maintain a good interface contact as before.

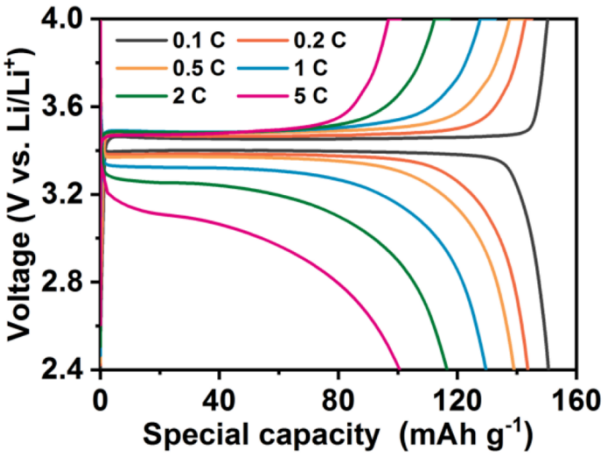

Fig. S13 The charge-discharge curves of $LiFePO_4$|PVDF-Li-LZ SSCEs|Li cell under different C-rates under 25 °C.

The $LiFePO_4$|PVDF-Li-LZ SSCEs|Li cell delivers the discharge capacity of 151 mAh g^{-1}, 144 mAh g^{-1}, 139 mAh g^{-1}, 130 mAh g^{-1}, 117 mAh g^{-1} and 101 mAh g^{-1} at 0.1 C, 0.2 C, 0.5 C, 1 C, 2 C and 5 C respectively (Fig. S13), among which the capacity retention at 5 C reaches up to 66.9%, demonstrating a far more excellent rate performance than that of the $LiFePO_4$/Li cells with PVDF-0.3Li SPEs, PVDF-Li SPEs or PVDF-Li-LZ SCEs.

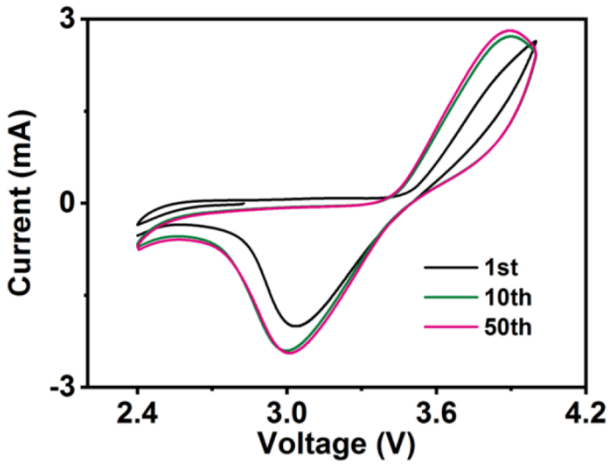

Fig. S14 The CV curves of $LiFePO_4$|PVDF-Li-LZ SSCEs|Li cell at a scanning speed of 10 mV s^{-1}.

As shown in Fig. S14, the CV curves of $LiFePO_4$|PVDF-Li-LZ SSCEs|Li cell from the beginning to the 50th cycle are well matched, indicating an outstanding electrochemical stability of PVDF-Li-LZ SSCEs.

References

1 X. Zhang, T. Liu, S.F. Zhang, X. Huang, B.Q. Xu, Y.H. Lin, B. Xu, L.L. Li, C.W. Nan, Y. Shen, Synergistic coupling between $Li_{6.75}La_3Zr_{1.75}Ta_{0.25}O_{12}$ and poly(vinylidene fluoride) induces high ionic conductivity, mechanical strength, and thermal stability of solid composite electrolytes, *J. Am. Chem. Soc.*, 2017, **139**, 13779-13785.

2 M.J. Lee, D.O. Shin, J.Y. Kim, J. Oh, S.H. Kang, J. Kim, K.M. Kim, Y.M. Lee, S.O. Kim, Y.G. Lee, Interfacial barrier free organic-inorganic hybrid electrolytes for solid state batteries, *Energy Stor. Mater.*, 2021, **37**, 306-314.

3 C.J. Bai, Z.G. Wu, W. Xiang, G.K. Wang, Y.X. Liu, Y.J. Zhong, B.T. Chen, R.D. Liu, F.R. He, X.D. Guo, Poly(ethylene oxide)/Poly(vinylidene fluoride)/$Li_{6.4}La_3Zr_{1.4}Ta_{0.6}O_{12}$ composite electrolyte with a stable interface for high performance solid state lithium metal batteries, *J. Power Sources*, 2020, **472**, 228461.

4 J.X. Zhang, N. Zhao, M. Zhang, Y.Q. Li, P.K. Chu, X.X. Guo, Z.F. Di, X. Wang, H. Li, Flexible and ion-conducting membrane electrolytes for solid-state lithium batteries: Dispersion of garnet nanoparticles in insulating polyethylene oxide, *Nano Energy*, 2016, **28**, 447-454.

5 W.Y. Liu, C.J. Yi, L.P. Li, S.L. Liu, Q.Y. Gui, D.L. Ba, Y.Y. Li, D.L. Peng, J.P. Liu, Designing polymer-in-salt electrolyte and fully infiltrated 3D electrode for integrated solid-state lithium batteries, *Angew. Chem. Int. Ed.*, 2021, **60**, 12931-12940.

6 J. Lu, Y.C. Liu, P.H. Yao, Z.Y. Ding, Q.M. Tang, J.W. Wu, Z.R. Ye, K. Huang, X.J. Liu, Hybridizing poly(vinylidene fluoride-co-hexafluoropropylene) with $Li_{6.5}La_3Zr_{1.5}Ta_{0.5}O_{12}$ as a lithium-ion electrolyte for solid state lithium metal batteries, *Chem. Eng. J.*, 2019, **367**, 230-238.